GEOMETRIC CALIBRATION FOR THERMOGRAPHY CAMERAS

Thomas SCHMIDT
German Aerospace Center, Institute of Structures and Design, Center for Lightweight-Production-Technology (ZLP), Am Technologiezentrum 4, 86159 Augsburg, Germany
Phone: +49-821-319874-1050; Mobile: +49-172-8343570; Fax: +49-8153-281028,
E-mail: t.schmidt@dlr.de

Christoph FROMMEL
German Aerospace Center, Institute of Structures and Design, Center for Lightweight-Production-Technology (ZLP), Am Technologiezentrum 4, 86159 Augsburg, Germany
Phone: +49-821-319874-1074
E-mail: christoph.frommel@dlr.de

Abstract. The application of active thermography applied as Lock-in or pulse thermography has been widely used in aerospace industry. Over the last years a number of activities had been undertaken to achieve a higher level of automation. Industrial robots are very versatile and allow a comparably easy integration of a measurement system in robotic workcell further the control unit. It is therefore possible to cover a large range of geometrical complex parts even on larger dimensions. The robot can be used for the positioning of the thermography camera and delivers the location of the robot flange coordinate system at the time of measurement automatically. In principle thermography cameras used in NDT applications as well as other fields can be handled as standard photogrammetric cameras. According to the longer wavelengths of the measured spectrum the lenses of thermography cameras are made of Germanium. Although the high cost for these lenses, they are optimized for radiometric resolution, thus geometric precision or minimal distortion are of minor interest.

The approach at DLR Augsburg of a robot based measuring system for industrial thermography applications and a hand-eye-calibration procedure for a thermography end-effector has been presented in previous papers. In order to achieve higher accuracy in terms of geometric precision a number of distortion parameters have been evaluated. An automated procedure has been developed to compare different calibration strategies. Within this paper DLR-Center for Lightweight-Production-Technology in Augsburg will give insight into current work in the area of geometric calibration for thermography cameras for a high resolution camera and results derived from experiments.

1 Introduction

A high level of automation is needed in today’s industrial manufacturing processes, hence require to automate the quality management behind the processes. Some examples have already been presented by DLR Augsburg in previous papers. A solution to do this is to measure defects with quality measuring tools mounted on a robot, see Figure 1. [1]

Figure 1 Automated testing using active thermography on an industrial robot

One of the methods that are used to measure the quality of a specimen is active thermography. At DLR Augsburg mainly the optical excited lock-in thermography is used. For this method a cooled thermography camera type FLIR Silver SC5600 is used. Unlikely to normal cameras thermography cameras aren’t geometrically calibrated by default. Consequential the images taken by thermography cameras reveal distortion. The distortions can be differentiated in pincushion or barrel distortion and as depicted in Figure 2.

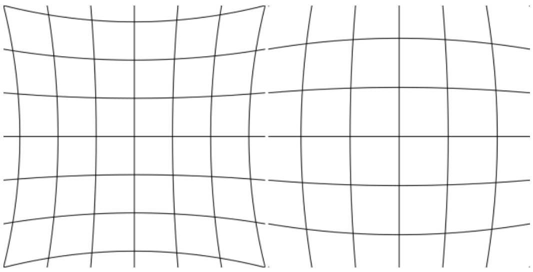

Figure 2 Distortion examples of different optical systems (e.g. pincushion (left), barrel distortion (right))

In order to achieve a correct sizing and locating of found defects in manufactured parts these distortions have to be determined and eliminated where possible. Therefore a calibration method has to be developed, deeply investigated and finally improved. Studies in other areas have identified the same circumstances but have chosen different approach to overcome this. [2]

1.1 Calibration Method

The calibration method that is currently used is derived from optical cameras and performed with an open camera calibration toolbox for Matlab® [3], [4]. The basic idea of this method is to take several images from a defined pattern at different angels and rotations but always with the same distance. The distance defines your focal length, which has to be always the same for each picture. For this toolbox two different patterns, the checkerboard and the point pattern, which can be seen in Figure 3 had been investigated.

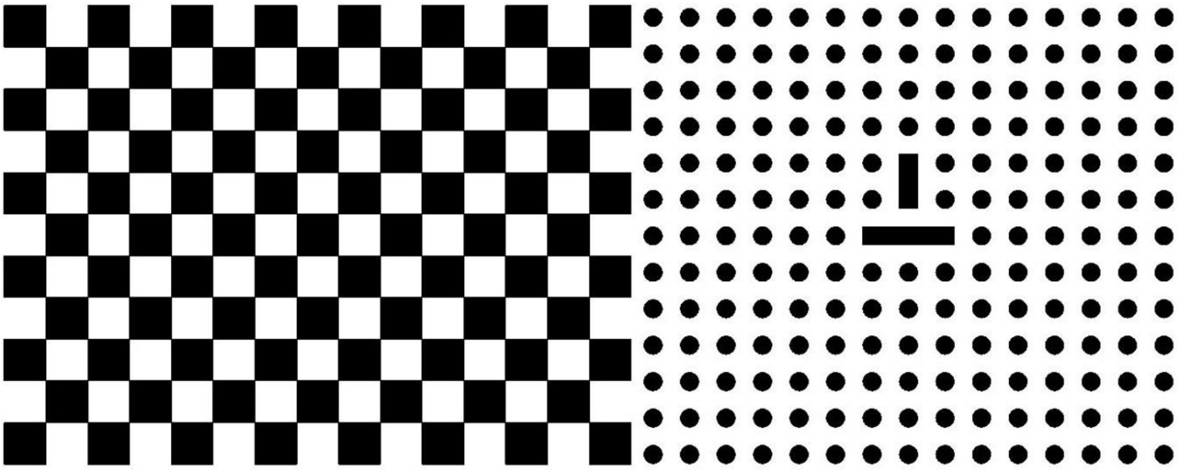

Figure 3 Calibration pattern examples (e.g. checkerboard (left), point pattern (right))

After the images were taken, the toolbox tries to fit grids, with the length of the checkers or the distance between two point centres, in the image and calculates camera parameters and distortion matrix. Also the field of view and the distortion model are calculated. With help of the camera matrix and the distortion matrix it is now possible to undistort the images for its respective working distance.

1.2 Main challenges

The first challenge that had to be solved was the correct generation of the patterns. The patterns have to be exactly the size you are telling the software to fit the grid on. Likewise the patterns have to be flat so that they don't amplify distortion.
The second challenge is the generation of a useful picture. An infrared camera produces images at room temperature that are very blurry as long as there are no temperature gradients, shown in Figure 4.

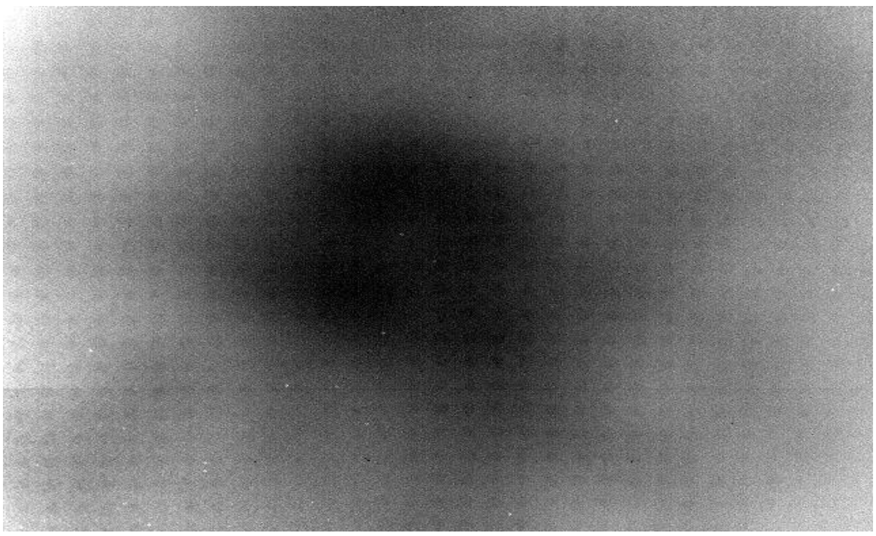

Figure 4 Image from point pattern taken from infrared camera at room temperature

Best results to overcome this issue had been achieved by applying active thermography, optically excited lock-in thermography in particularly using the inverted amplitude image. The thermography results depend on the excitation frequency, magnitude of the halogen lamps, transient oscillation periods and measurement periods. Also the patterns need to have a thermic behaviour that is suitable for the lock-in thermography. That means that they should not reflect or disturb the thermography to generate good quality images. To ensure the measurements were reproducible a defined experiment set up had to be configured. This also is needed to compare the different patterns to each other.

2 Experiments

The experiments can be divided in two parts. The first was the installation of the experimental set-up. The second one was the execution of the experimental set-up.

2.1 Experimental set-up

Two different types of lenses were available and suspect to be characterised. The first lens (A) is a wide-angle lens with 12 mm focal length. The second one (B) has a focal length of 27 mm. For both lenses the working distances had to be found. A decision had been made to progress the experiments on 5 "working distances", the lens position ("Brennweitenposition") BWP had been monitored. The results are listed in Table 1.

Table 1 Working distances and image size

Lens A			Lens B		
Working distance [mm]	BWP	Image size [mm x mm]	Working distance [mm]	BWP	Image size [mm x mm]
100	3440	116 x 92	200	4714	82 x 61
300	2859	297 x 225	550	2557	207 x 166
500	2704	465 x 358	850	2203	312 x 255
700	2686	615 x 497	1200	1995	435 x 347
900	2649	785 x 610	1500	1821	550 x 435

With this information the size of patterns had been determined and the layout of the pattern was created. The pattern had been printed using a commercial inkjet plotter and finally bonded on ALU-Dibond. By finishing the patterns the experimental set-up could be assembled. The thermography system from DLR Augsburg was used to acquire the images. As energy source halogen lamps were used. A CNC gantry with a mounted rotary tilting unit had been used to manipulate the patterns. This method led to 12 pictures including the same "randomness" for each calibration to ensure comparability. One of the experimental set-ups can be seen in Figure 5.
With the experimental set-up finished the parameters of the lock-in thermography could be determined. On such experimental set-up a high magnitude in combination with a relatively high excitation frequency, one transient oscillation period and 3 measurement periods, visualized in the amplitude image of the lock-in thermography, were giving the best quality images.

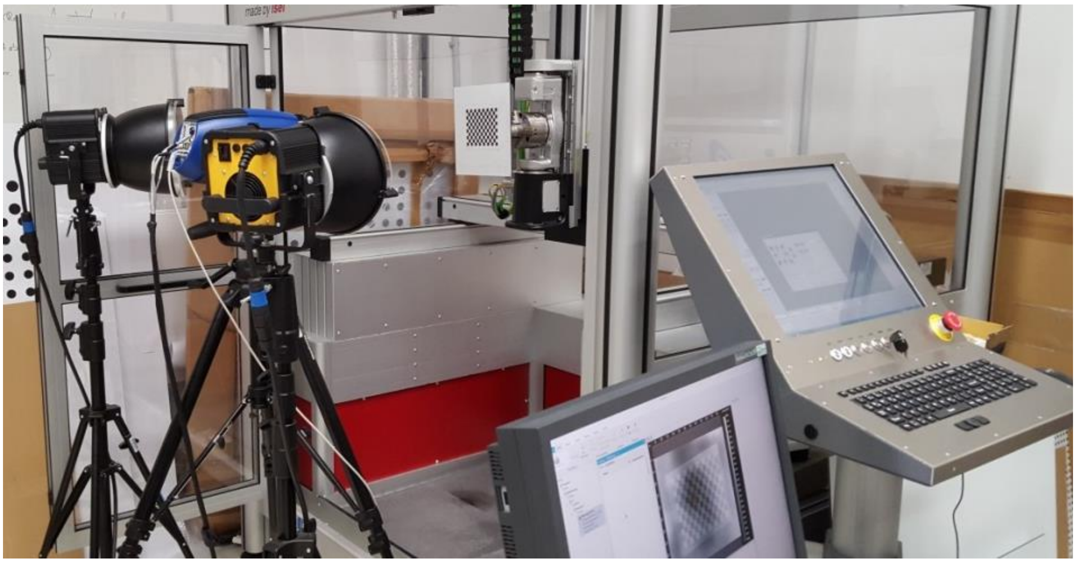

Figure 5 Experimental Set-Up

2.2 Test execution

To ensure comparability of each measurement the procedure was always the same. From now on only the CNC portal had to be adjusted to the set-up and for each position the measurement was taken until all 12 positions were captured. One of these pictures is shown in Figure 6 and the distortions can be clearly seen.

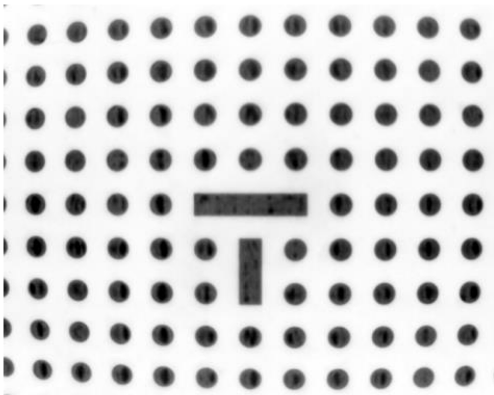

Figure 6 Example calibration image from point pattern with strong distortions

3 Camera calibration

To demonstrate the procedure the calibration for working distance 500 mm for lens A will be shown. The images from thermography can be loaded in the memory of the calibration which can be seen in Figure 7.

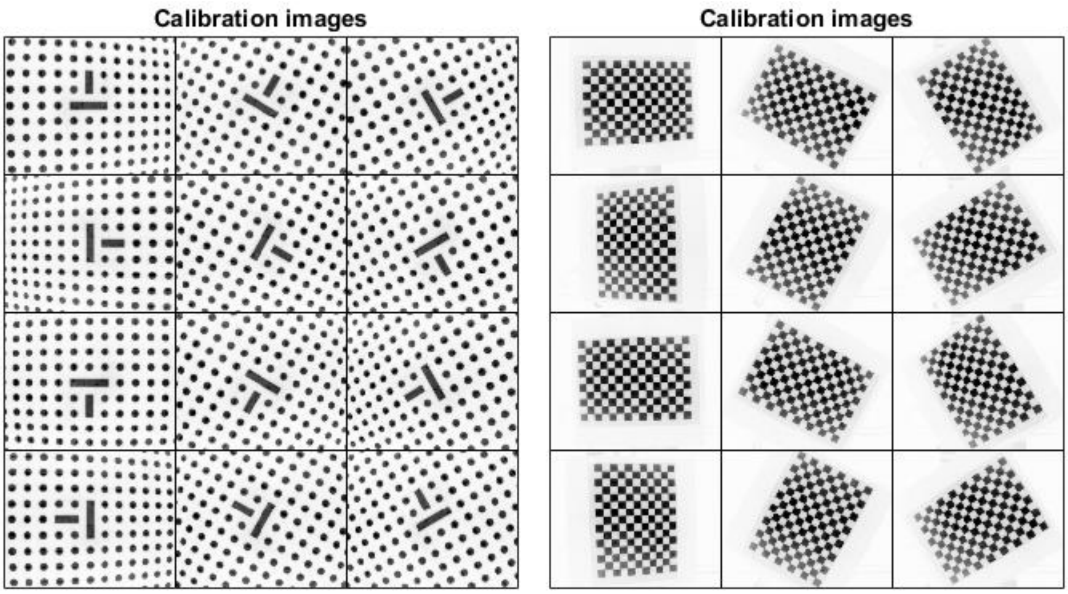

Figure 7 Calibration images for both patterns (point pattern (left), checkerboard (right))

So that the toolbox knows the size of the pattern the distance in x-direction and y-direction between the centres of two points respectively the edge length of the checkers must be entered in millimetre. In a first step the toolbox estimates some of the values like the principal point, which is the point on the sensor of the camera in pixel where the lens projects the image in reality. After the first run with these assumptions a second iteration is done to generate the real parameters of the calibration which can be found in Table 2. The both patterns are slightly different in user interaction and produce different results as we will discuss later in this study.

Table 2 Calibration results

Focal Length:	[779,04243 777,89253] ± [4,61134 4,50278] mm
Principal point:	[311,56490 253,30857] ± [1,28949 1,06870] px
Skew:	[0 0 90 0]
Distortion:	[-0,27219 0,13748 -0,00033 0,00007 0] ± [0,00728 0,03761 0,00028 0,00028 0]
Pixel error:	[0,09323 0,08840] px

The first parameter achieved is the focal length in mm for horizontal and vertical direction. Second the principal point in pixel is given. The third value called skew describes the angle of the pixels. For our measurements all pixel were rectangular so this value was not changed in the calibration. With these 3 values the so called camera matrix KK can be written as follows:

$$KK = \begin{bmatrix} 779{,}04243 & 0 & 311{,}56490 \\ 0 & 777{,}89253 & 253{,}30857 \\ 0 & 0 & 1 \end{bmatrix}$$

In correlation with the distortion vector the images can be undistorted by the toolbox. Using all this information, camera matrix KK, the toolbox will be able to reproject the points of the input images to their respective grid position which is visible in Figure 8. The blue vectors describe the movement of the point that has to be done to move him in his perfect grid position at a maximum of 0,25 pixel. On the right side of Figure 8 the error that occurs during this process of every input image is shown.

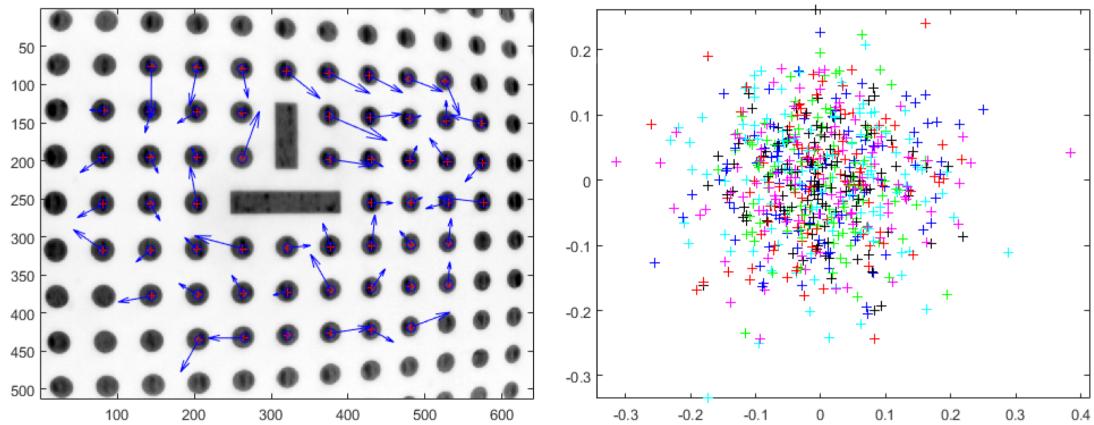

Figure 8 Reprojection errors (vector plot for single image (left), XY plot for all calibration images (right))

The last feature of the toolbox is the visualization of the distortion of the image. The complete distortion model can be divided in radial and tangential distortion. The radial and tangential distortion can be found in Figure 9.

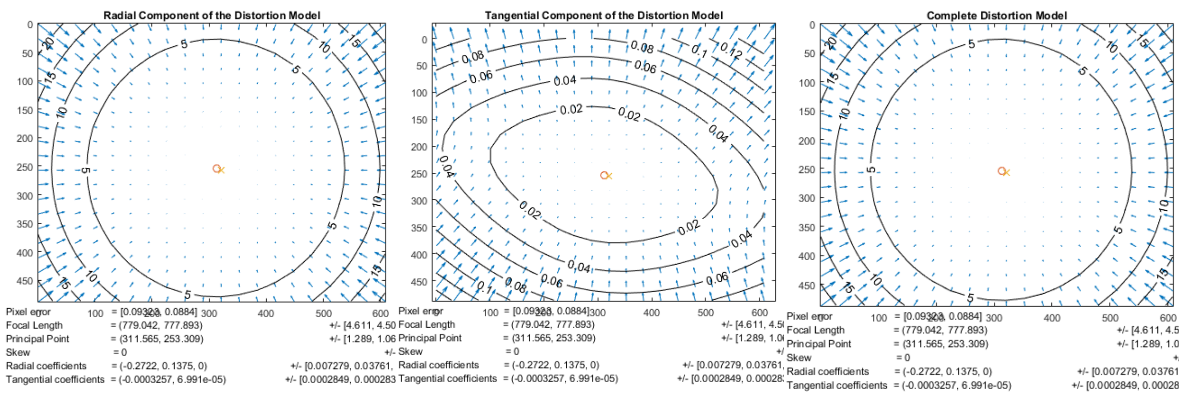

Figure 9 Distortion components, radial component (left), tangential component (middle), complete distortion model (right)

For our lens the tangential distortion is extremely low which means that the plane of the lens is almost perfect parallel to the sensor of the camera and is for our case negligible [5]. This also is shown in the complete distortion model Figure 9, because it is almost the same as the radial distortion model. Finally each image can be visualized undistorted, differences can be seen in Figure 10. You can also see that the barely visible points on the left side disappear in the undistorted image because of its decrease in height and width.

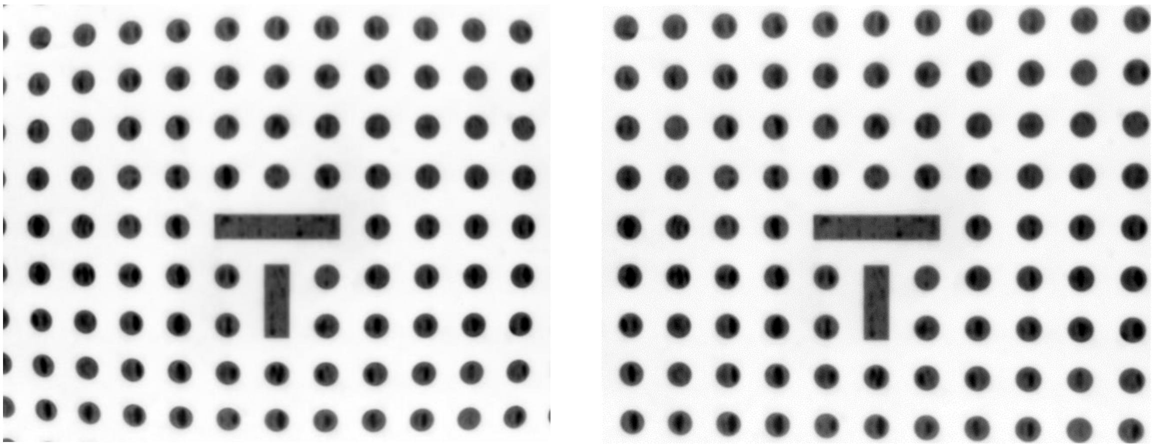

Figure 10 Distorted image (left), undistorted image (right)

4 Discussion of results

An important part of evaluation is the difference between the two patterns. For lens A the values don't differ much and are almost the same within its error range which can be seen in Figure 11. For lens B however the first working distance shows different values. Since the errors of both patterns are very high at this working distance we assume that it is too close to the camera and not within a reasonable working range. Over all the errors for the two lenses show that the point pattern has less error in its calibration. They also show that the errors for lens B is about 4 times higher than for lens A. The error of the checkerboard pattern is about 20% higher than the point pattern. Only for the focal length of lens B the error is almost twice as high. The high error results from the lesser area of the checkerboard pattern that is covering the image.

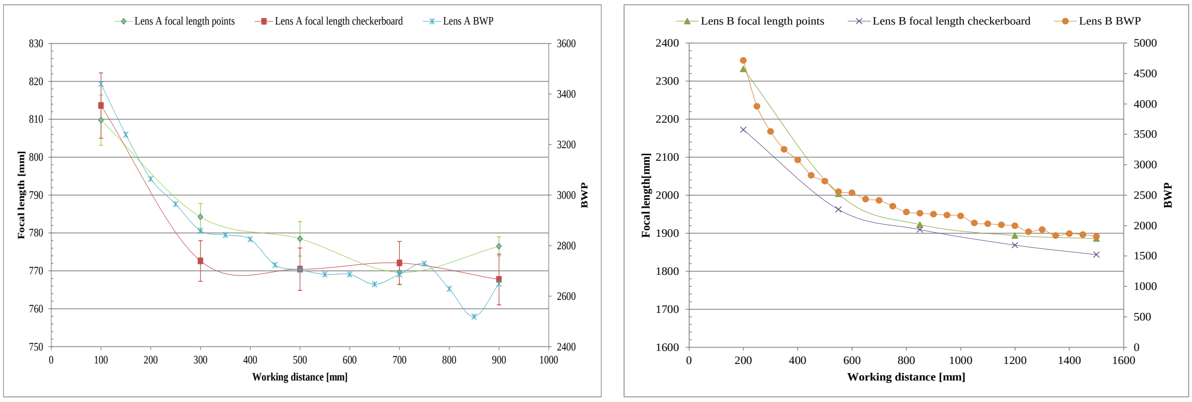

Figure 11 Comparison of calibration results lens A and B

In Figure 11 also the BWP is shown. Here you can see that the trend is the same as the focal length. Since the BWP is the only value we get from the camera that defines the working distance, this now sets a correlation to the calibration. Finally for the checkerboard pattern the experimental set-up is much easier, but the point pattern is the better choice for the thermography camera calibration revealing higher precision at similar effort.

After the calibration for each pattern was done, a way to evaluate the quality of calibration had to be found. Therefor the undistorted images had been used for another calibration, delivering distortion coefficients close to zero, see Table 3:

Table 3 Calibration parameters of second calibration

Focal Length:	[778,78719 777,59995] ± [4,07707 3,97590] mm
Principal point:	[312,29279 253,45963] ± [1,07206 0,88134] px
Skew:	[0 0 90 0]
Distortion:	[0,00339 -0,02767 -0,00018 -0,00009 0,00000]±[0,00601 0,03102 0,00036 0,00045 0,00000]
Pixel error:	[0,09841 0,09637] px

5 Conclusions

Within this study the quality of images taken for calibration had been improved drastically. With variations in the pattern type the calibration itself could be investigated in errors and circumstances. Also relations between working distance and calibration parameters like focal length could be found. Therefore a better localisation of the defects shown on the images is given. Knowing that the point pattern is giving better results, the error produced by these measurements could even be minimized by taking more pictures at each working distance. Also the dependency on the working distance could be investigated by adding several distances to the calibration. Because the calibration parameters are dependent on the working distance the calibration for each distance has to be done. An optimisation would be a graph in which you can choose your calibration parameters dependent on the BWP. If this graph would be achievable by making experimental set-ups with reasonable effort it would reduce the amount of calibrations that have to be done drastically.

6 Acknowledgements

This work had been founded by the state government of Bavaria, the city of Augsburg and DLR and the initial funding of the start-up project of the Center for Lightweight-Production-Technology (ZLP). Special thanks go to team members of ZLP Augsburg.

7 References

[1] T. Schmidt, „Hand-eye-calibration of a robotized thermography end-effector,“ *NDT in Aerospace 2014,* 06 10 2014.

[2] T. Luhmann, J. Ohm, J. Piechel and T. Roelfs, "Geometric Calibration of Thermographic Cameras," in *International Archives of Photogrammetry, Remote Sensing and Spatial Information Sciences, Vol. XXXVIII, Part 5,* Newcastle upon Tyne, UK, 2010.

[3] J.-Y. Bouguetj, "Camera Calibration Toolbox for Matlab," [Online]. Available: http://www.vision.caltech.edu/bouguetj/calib_doc/. [Accessed 10 2013].

[4] E. Zurich, "Fully automatic camera and hand to eye calibration," [Online]. Available: https://www.vision.ee.ethz.ch/software/calibration_toolbox/calibration_toolbox.php. [Accessed 10 2013].

[5] o. d. team, “OpenCV 2.4.9.0 documentation,” 2014. [Online]. Available: http://docs.opencv.org/doc/tutorials/calib3d/camera_calibration/camera_calibration.html. [Accessed 07 2014].